

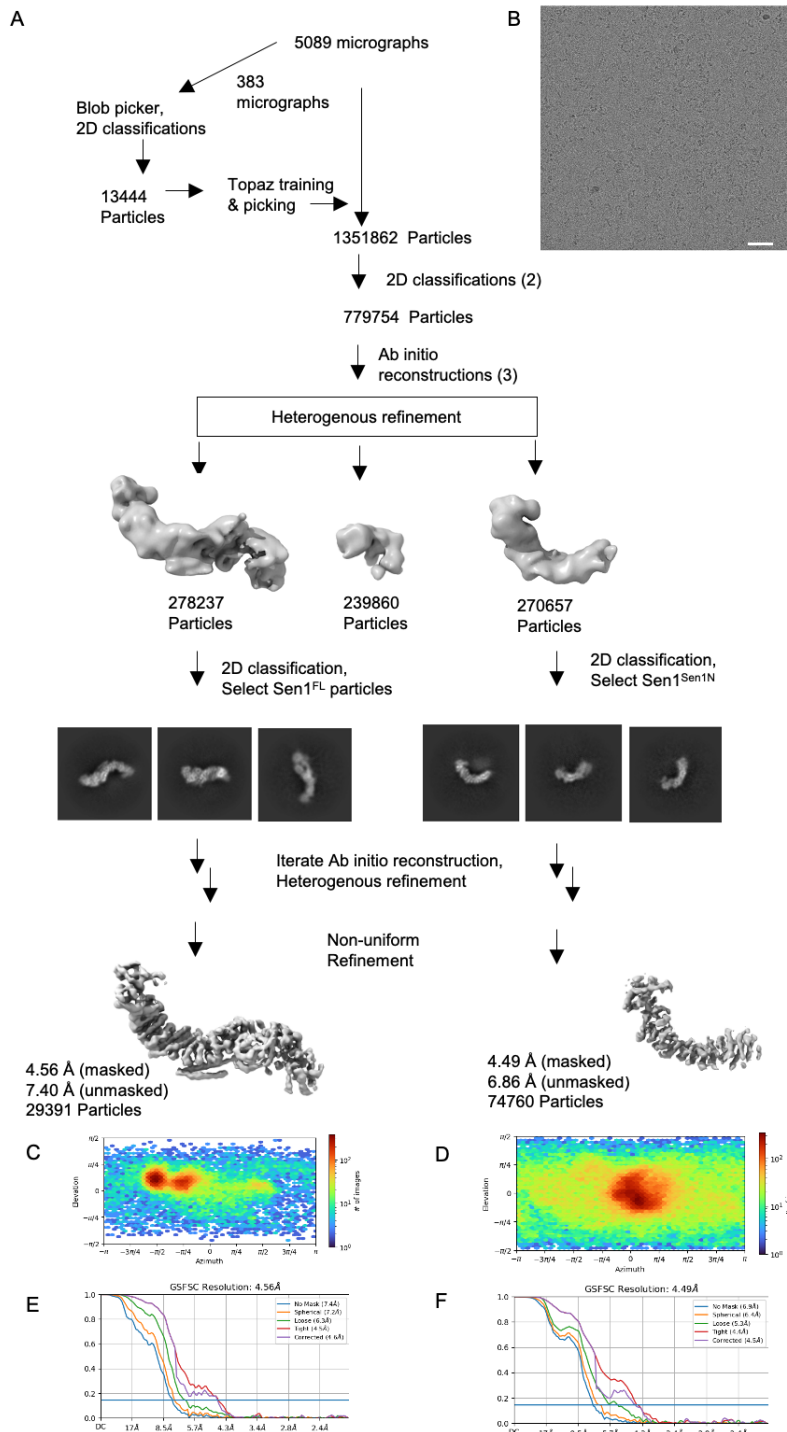
Supplementary Figure 1. Purification and characterization of *Chaetomium thermophilum* Sen1, Related to STAR methods

(A) Domain architecture of CtSen1. Brown lines mark boundaries of trypsin stable domains.

(B) Purification scheme for YFP-CtSen1. Anti-GFP nanobody conjugated sepharose resin binds tightly to YFP-CtSen1. The purified protein is released from the column by overnight cleavage with TEV-protease, and subsequently purified by size-exclusion and ion exchange chromatography. Representative gels of the TEV elution, ion exchange and SEC, and purified protein are shown.

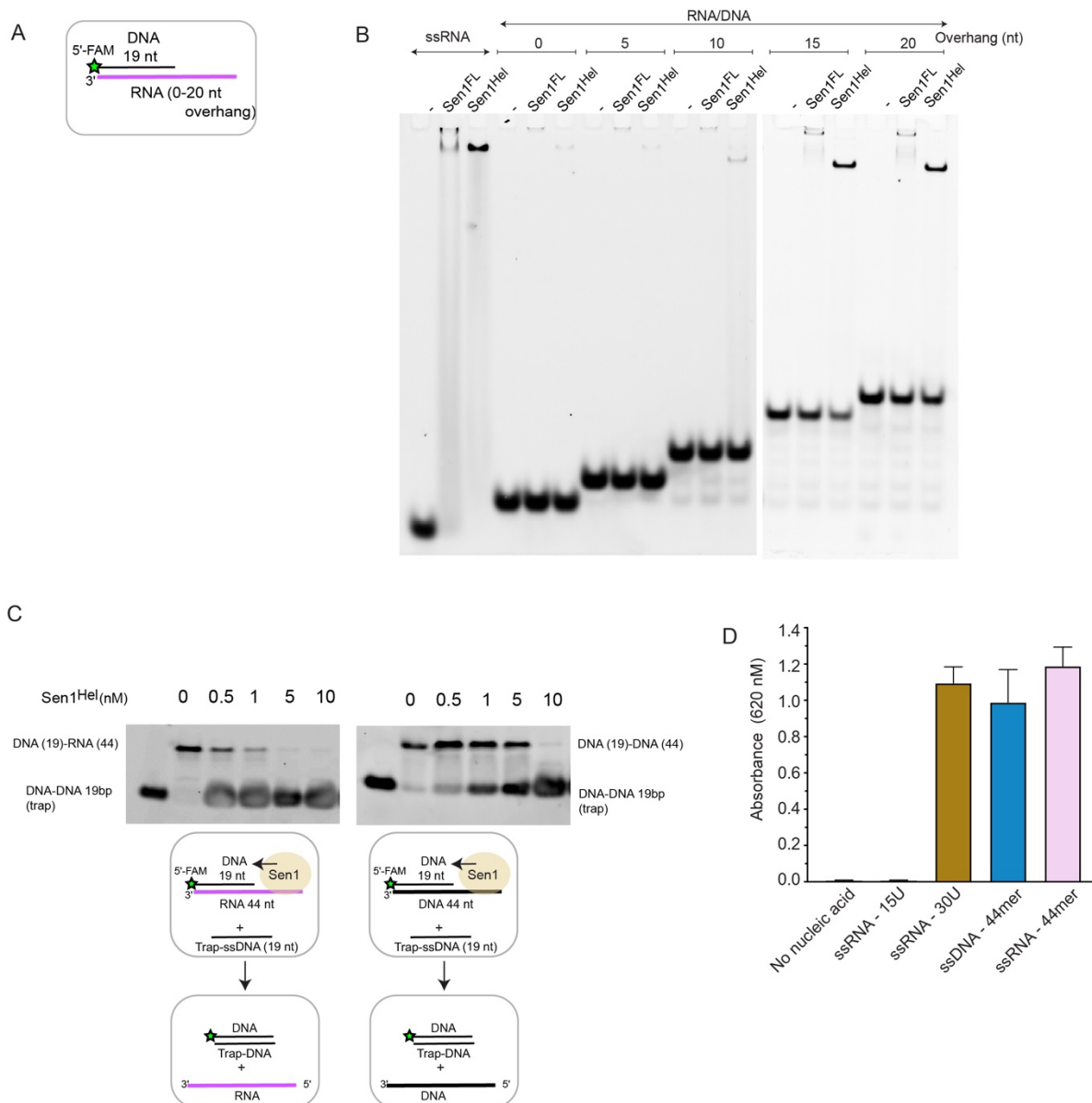
(C) Limited trypsin proteolysis of CtSen1^{FL} yields two stable Sen1 domains.

(D) IUPred (Dosztanyi et al., 2005) disorder plot of CtSen1 shows two structured regions of the protein map to the N- and C-terminal domains defined by tryptic proteolysis.



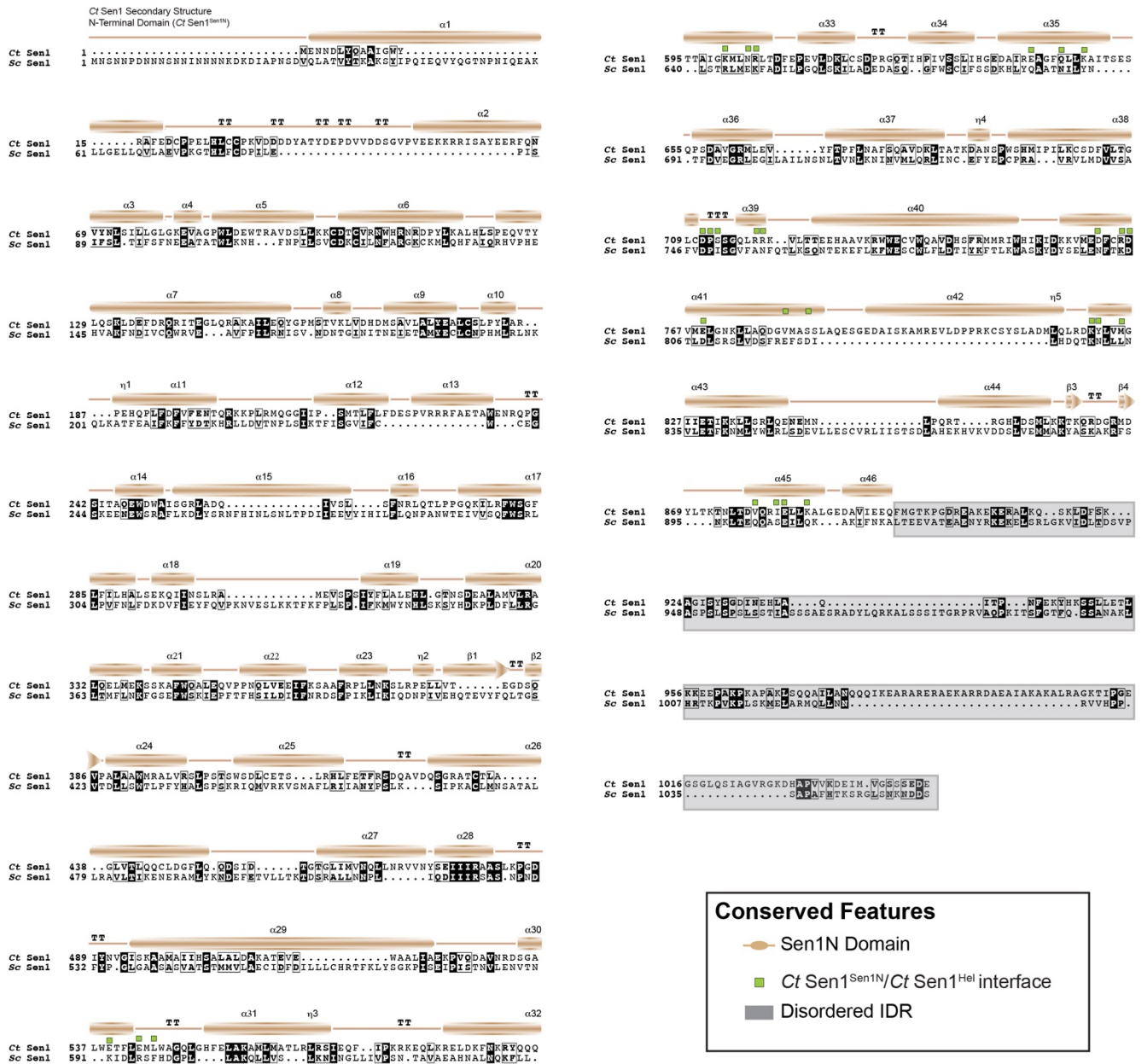
Supplementary Figure 2. Cryo-EM data collection and processing for Sen1^{FL} and Sen1^{Sen1N}, Related to Figure 1 and STAR methods

- (A) Flowchart of CryoSPARC image processing for Sen1^{FL}
- (B) Example micrograph of Sen1^{N-PP-C}. Scale bar 20 nm.
- (C) Angular distribution plot of particles used in the Sen1^{FL} reconstruction.
- (D) Angular distribution plot of particles used in the Sen1^{Sen1N} reconstruction.
- (E) Fourier Shell correlation for the Sen1^{FL} reconstruction.
- (F) Fourier Shell correlation for the Sen1^{Sen1N} reconstruction.



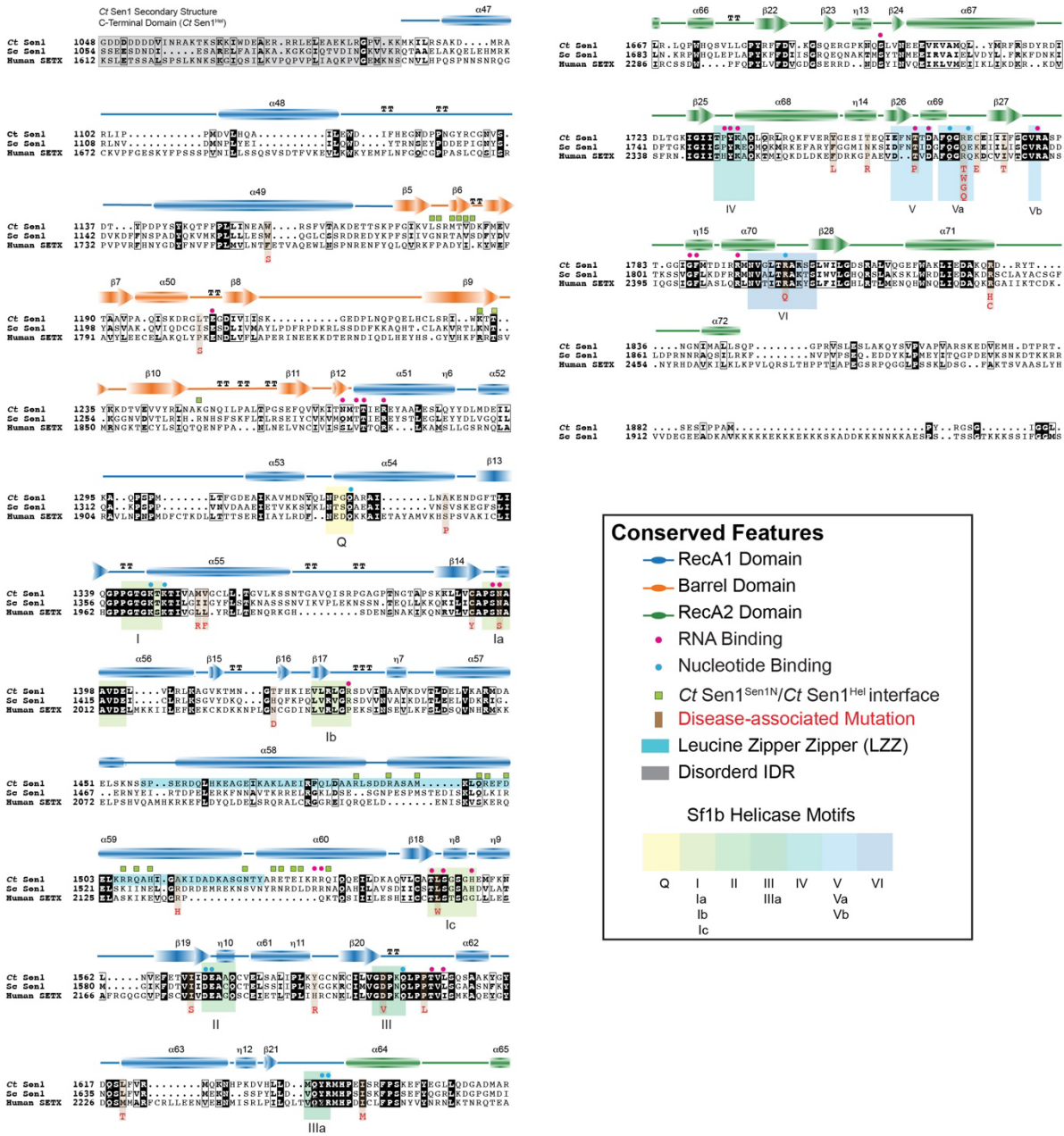
Supplementary Figure 3. RNA-DNA binding and helicase activity of Sen1^{FL} and Sen1^{Hel}, Related to Figure 2 and STAR Methods

- (A) EMSA substrates for assays shown in panel “b” vary the length of RNA overhang.
 (B) EMSA analysis of Sen1^{FL} and Sen1^{Hel}. RNA-DNA substrates (10 nM, Sub1-Sub4) were incubated with Sen1^{FL} (50 nM) or Sen1^{Hel} (50 nM) on ice for 15 min. Samples were resolved on 6% TBE gels and FAM-labeled reaction products were visualized on a Typhoon FLA 9000 scanner (GE Healthcare).
 (C) Sen1^{Hel} activity on RNA-DNA hybrid (left) versus and equivalent DNA-DNA duplex (right).
 (D) Sen1^{Hel} (5 nM) was incubated with 15U-RNA, 30U-RNA, 44-DNA and 44-RNA (Supplementary Table 4) at 5 μ M and ATP (1 mM) for 15 min at 37°C. The hydrolysis products were detected using colorimetric Malachite Green Phosphate Assay Kit. Absorbance was measured at 620 nm.



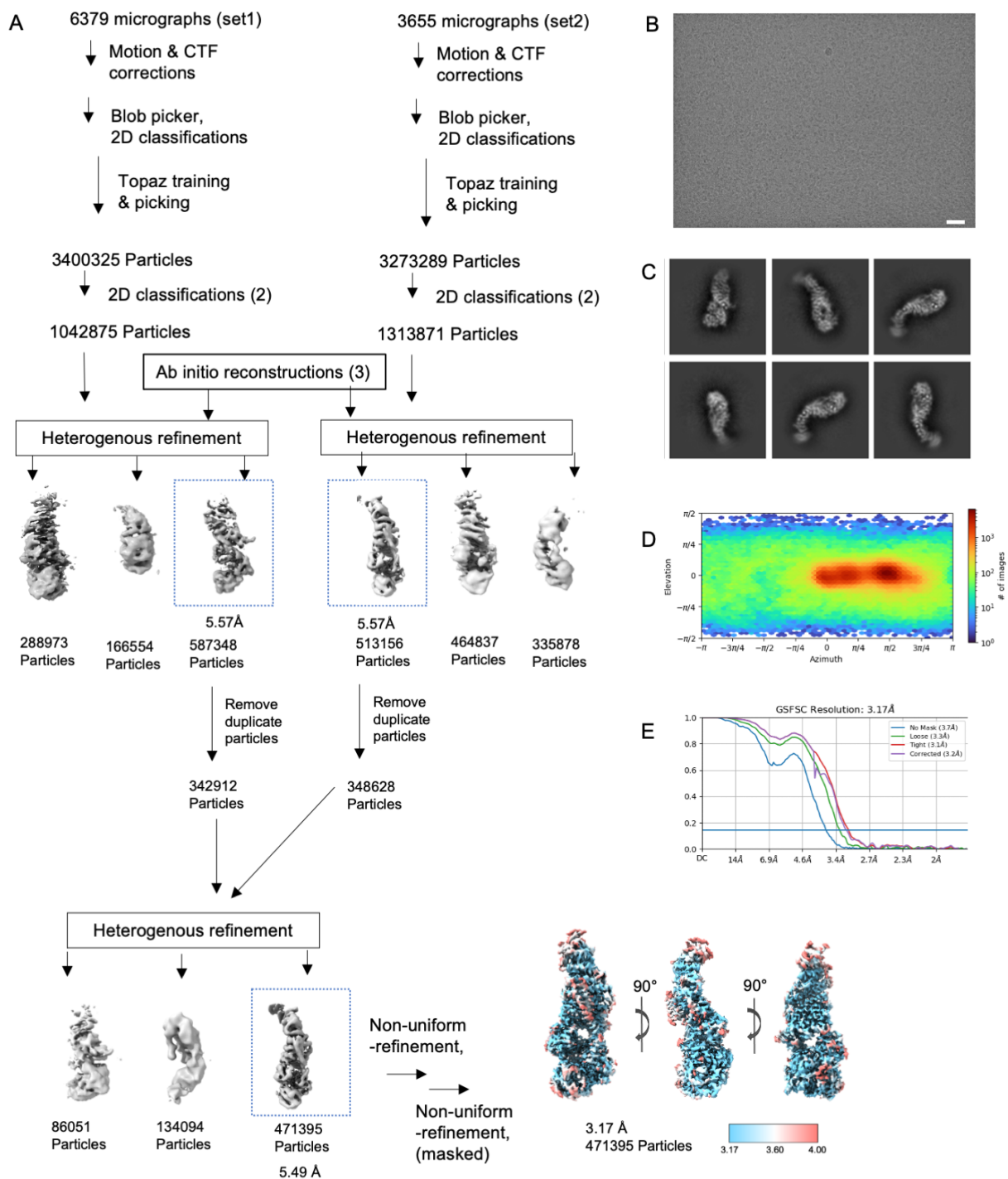
Supplementary Figure 4. CtSen1 sequence alignments, Related to Figure 2

Sequence alignment of the Sen1 amino terminal Sen1N region. Alignments were generated in ClustalW, rendered within Esript, and annotated in Adobe Illustrator. Secondary structure from Esript is noted, TT= tight turn.



Supplementary Figure 5. CtSen1 sequence alignments, Related to Figure 2

Sequence alignment of the Sen1 helicase domain. Alignments were generated in ClustalW, rendered within Espritt, and annotated in Adobe Illustrator. Secondary structure from Espritt is noted, TT= tight turn.



Supplementary Figure 6. Cryo-EM data collection and processing for Sen1^{N-PP-C}, Related to Figure 5

- (A) Flowchart of CryoSparrc image processing for Sen1^{N-PP-C}.
- (B) Example micrograph of Sen1^{N-PP-C}. Scale bar 20 nm.
- (C) Representative 2D class averages of Sen1^{N-PP-C}.
- (D) Angular distribution plot of particles used in the Sen1^{N-PP-C} reconstruction.
- (E) Fourier Shell correlation for Sen1^{N-PP-C}.

Supplementary Table 1. AOA2 and ALS4 mutations in Sen1 helicase domain, Related to Figure 7

Domain	Human SETX*	ScSen1	CtSen1	Disease	Possible Structural Impacts
Helicase	F 1756 S	W 1166 S	W 1158 S	AOA2	Folding
Helicase	P 1805 S	V 1205 S	L 1203 S	AOA2	RNA binding, Folding
Helicase	A 1945 P	S 1346 P	L 1329 P	AOA2	Folding
Helicase	L 1976 R	I 1370 R	M 1353 R	AOA2	Folding
Helicase	L 1977 F	I 1371 F	V 1354 F	AOA2	Folding
Helicase	C 2006 Y	C 1409 Y	C 1392 Y	AOA2	RNA Binding, Folding
Helicase	N 2010 S	N 1413 S	N 1396 S	AOA2	RNA binding
Helicase	N 2037 D	H 1433 D	T 1406 D	AOA2	Folding
Helicase	R 2136 H R 2136 C	D 1550 H D 1550 C	K 1532 H K 1532 C	ALS4 ALS4	RNA/DNA hybrid binding
Helicase	L 2155 W	L 1569 W	L 1551 W	AOA2	RNA binding/Folding
Helicase	I 2179 S	I 1588 S	I 1570 S	AOA2	Folding
Helicase	H 2197 R	Y 1606 R	Y 1588 R	AOA2	Folding
Helicase	D 2207 V	D 1616 V	D 1598 V	AOA2	ATP binding/hydrolysis
Helicase	P 2213 L	P 1622 L	P 1604 L	AOA2	RNA binding
Helicase	M 2229 T	L 1638 T	L 1620 T	AOA2	Folding
Helicase	I 2264 M	I 1661 M	I 1645 M	AOA2	Folding
Helicase	F 2363 L	F 1767 L	Y 1749 L	AOA2	Folding, Surface binding site
Helicase	P 2368 R	N 1772 R	T 1754 R	AOA2 AOA2	Folding, Surface binding site
Helicase	T 2373 P	T 1779 P	T 1761 P	AOA2	RNA binding
Helicase	R 2380 T R 2380 W R 2380 G R 2380 Q	Q 1786 T Q 1786 W Q 1786 G N/A	R 1768 T R 1768 W R 1768 G R 1768 Q	AOA2 AOA2 AOA2 AOA2	Protein folding, conformational change
Helicase	K 2382 E	K 1788 E	C 1770 E	AOA2	Protein folding, conformational change
Helicase	I 2386 T	L 1792 T	I 1774 T	AOA2	Folding
Helicase	R 2414 Q	R 1820 Q	R 1801 Q	AOA2	ATP binding/hydrolysis
Helicase	R 2444 H R 2444 C	R 1850 H R 1850 C	R 1831 H R 1831 C	AOA2 AOA2	Folding

[S1],[S2]

- S1. Chen Y. Z., Bennett C. L., Huynh H. M., Blair I. P., Puls I., et al., (2004). DNA/RNA helicase gene mutations in a form of juvenile amyotrophic lateral sclerosis (ALS4). *Am. J. Hum. Genet.* 74, 1128–1135.
- S2. Chen, X., Muller, U., Sundling, K.E., and Brow, D.A. (2014). *Saccharomyces cerevisiae* Sen1 as a model for the study of mutations in human Senataxin that elicit cerebellar ataxia. *Genetics* 198, 577-590. 10.1534/genetics.114.167585.